# Electrodeposition of Ni/Cu Multilayers

N.V. Myung & K. Nobe

**Nickel/copper multilayers have been electrodeposited from sulfamate baths containing nickel and copper ions by alternating potential pulses. Different electrochemical transient techniques were employed to investigate the electrodeposition of nickel and copper. In copper-free nickel sulfamate baths, nucleation of hemispherically shaped nickel proceeded initially under electron transfer control. The growth rate of nuclei increased exponentially with potential from 1 nm/sec at -0.895 V to 50 nm/sec at -1.3 V. At applied potentials more negative than -1.3 V, nickel hydroxide formed on the surface with nickel electrodepositing in the film cracks along with a small amount of α and β nickel hydrides because of high surface pH.**

**In the presence of copper ions, pure copper electrodeposits between -0.05 to -0.8 V. Copper deposition was under mass transfer control below -0.25 V because of low copper ion concentrations. Nickel codeposits with copper at potentials more negative than -0.85 V. The relative amount of copper codeposited with nickel decreased with decreasing potential. Current transient behavior of nickel also changed as a result of copper codeposition.**

**Nano-thick Ni/Cu multilayers were electrodeposited on platinum and on sputtered gold silicon. The optimum deposition potential range for nickel was between -1.20 and - 1.25 V to minimize the copper content and to prevent formation of nickel hydroxide and nickel hydride. The optimum deposition potential range for copper was between -0.4 and -0.8 V. The optimum thickness for Ni and Cu layers was approximately 10 and 0.5 nm, respectively. Electrical resistivity increased with increasing nickel thickness and decreasing copper thickness. X-ray diffraction patterns show good crystallinity of the Ni/Cu multilayers, where the preferred orientation of Ni/Cu multilayers was (200). SEM showed good lamellar Ni/Cu multilayers.**

Investigations of nano-structured materials increased rapidly in the 1990s because of their potential for enhancing mechanical, electrical, optical and magnetic bulk properties. Ultra high hardnesses of ceramic and metallic multilayered materials and high tensile strength and wear resistance of metallic multilayers are a few examples.[1] In 1989, a new magnetoresistance (MR) phenomenon called giant magnetoresistance (GMR) was discovered by Baibich *et al.* in nano-structured multilayers containing alternating magnetic (Fe) and non-magnetic (Cr) multilayers.[2] MR is the change of electrical resistance by the presence of an external magnetic field. The discovery of GMR opened up a new era of magnetic read heads.

Electrodeposition and electroless deposition processes, and vacuum deposition processes (sputtering, evaporation, chemical vapor deposition) have been used to deposit nano-structured films. Each has advantages for specific applications. Some limitations to the use of vacuum deposition processes, however, include high capital costs of vacuum equipment and high energy costs because of elevated deposition temperatures, whereas electrodeposition equipment costs are much less and operating temperatures range from room temperature to < 100 °C. Electrodeposition is an old and versatile technology that has wide applicability in various industries, including aircraft/aerospace, automotive, household appliances, and electronics, among others, because of its many advantages over other deposition technologies, namely, precisely controlled room temperature operation, lower energy requirements, faster deposition rates, deposition over

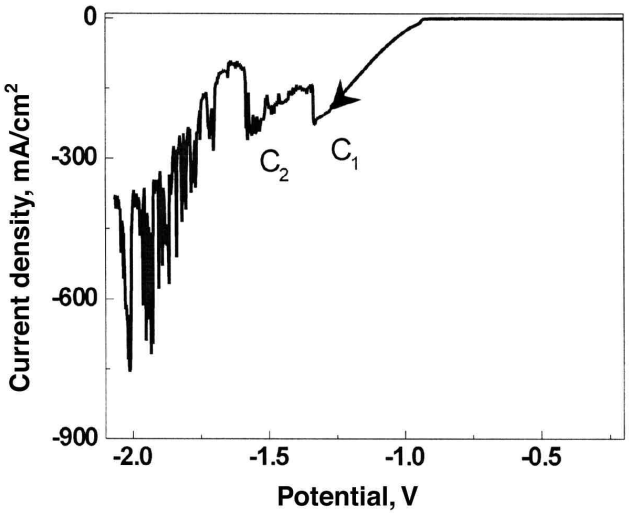


*Fig. 1—Linear cathodic potential sweep of platinum in 1.5 M Ni($H^2NSO_3$)$_2$ and 0.5 M $H_3BO_3$ at 5 mV/sec.*

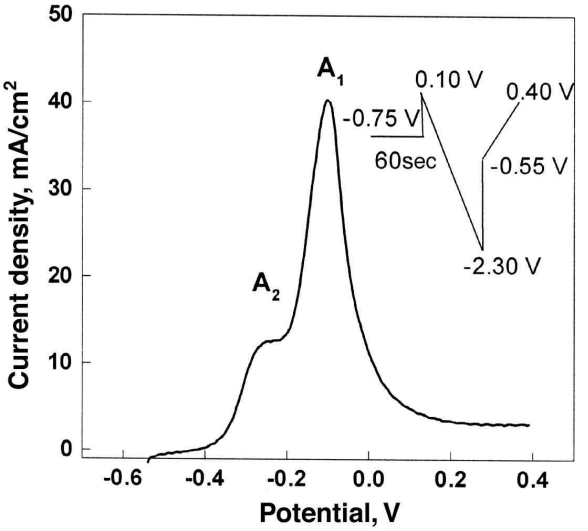


*Fig. 2—Potentiodynamic behavior of platinum in 1.5 M Ni($H_2NSO_3$)2, 0.5 M $H_3BO_3$ (Bath #1) at 1 mV/sec with perturbation program A.*

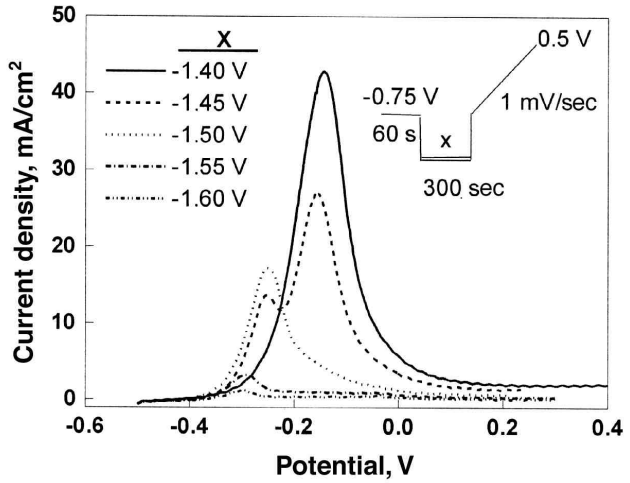


*Figure 3. Potentiodynamic behavior of platinum in 1.5 M $Ni(H_2NSO_3)_2$ and 0.5 M $H_3BO_3$ (Bath #1) at 1 mV/sec with perturbation program B.*

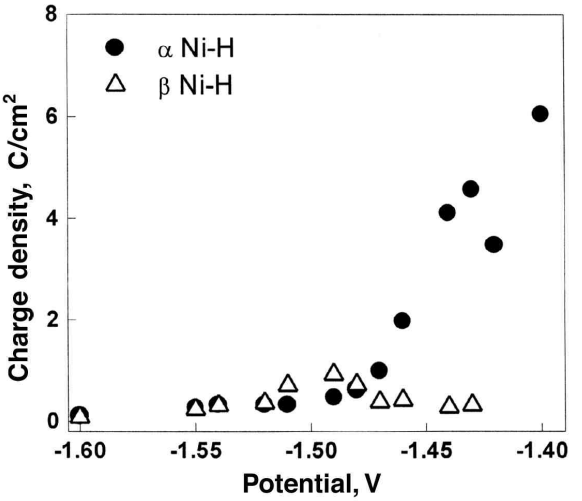


*Fig. 4—Anodic stripping charge of α- and β-nickel hydrides as a function of deposition potential.*

complicated shapes, deposition of binary, ternary and quaternary alloys over a wide range of compositions, structures and magnetic properties, and less costly and easily maintained equipment. The composition, structure and properties, including magnetic properties, of electrodeposited metals and alloys can be "tailored" by controlling deposition conditions and solution compositions.[3-5] By proper choice of deposition variables, it is possible to obtain a wide variety of alloy compositions and microstructures. The ability to electrodeposit films at room or slightly elevated temperatures is particularly important if the substrate is heat sensitive, as is frequently the case in electronic applications.

Two distinct methods, single-bath and dual-bath, have been used to electrodeposit multilayers. For the former, deposition is carried out in a single electrolyte by periodically varying deposition parameters, such as potential or current to produce multilayers.[6] For the latter, the substrate is transferred between two different electrolytes and the separate layers are deposited alternatively from each electrolyte. The single-bath technique has advantages and disadvantages over the dual bath technique. One advantage is that transferring the cathode from one bath to another is avoided and reduces possible contamination and oxide formation. The single bath technique requires, however, that all metal ions are contained in a single bath, creating the problem of codeposition of the two metals when the applied potential is below the deposition potential of the less noble metal. Most experimenters minimize this problem by increasing the ratio of the less noble metal ions to the more noble metal ions in the electrolyte. The codeposition problem still exists, however.

Different multilayers, including Ni/Cu, CoNi/Cu, Co/Cu, Fe/Cu, Co-Ni-W/Cu, and $N_{80}Fe_{20}$/Cu have been successively obtained by electrodeposition.[7,8] Bennett *et al*.[9] observed that electrodeposited multilayers had higher magnetic saturation ($B_s$) than vacuum-deposited films. Tench and White, and Menezes and Anderson showed enhancement in tensile strength of nano-structured Ni/Cu multilayers compared to bulk alloys.[10,11] The tensile strength of electrodeposited Ni/Cu was also superior to vacuum-deposited films.

Two different plating solutions have been used to electrodeposit Ni/Cu multilayers using the single bath technique. One was a modified Watts bath with addition of copper sulfate,[12,13] and the other was a nickel sulfamate bath with copper sulfate.[7,10,11,14-17] Both baths contained boric acid. For substrates, (100) and (111) orientations, or polycrystalline copper were used most often.[7,10-12,14-17] The kinetics of nickel electrodeposition on copper from nickel sulfamate baths containing copper sulfate is not well understood, however,

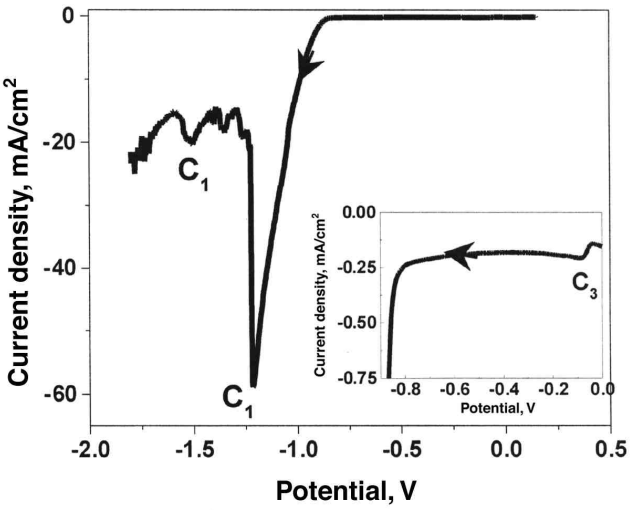


*Figure 5—Linear cathodic potential sweep of copper in 1.5 M $Ni(H_2NSO_3)_2$, 0.5 M $H_3BO_3$ and 1,000 ppm $CuSO_4$ (Bath #2) at 5 mV/sec. Inset is expanded scale of linear cathodic potential sweep: -0.85 < E < -0.00 V.*

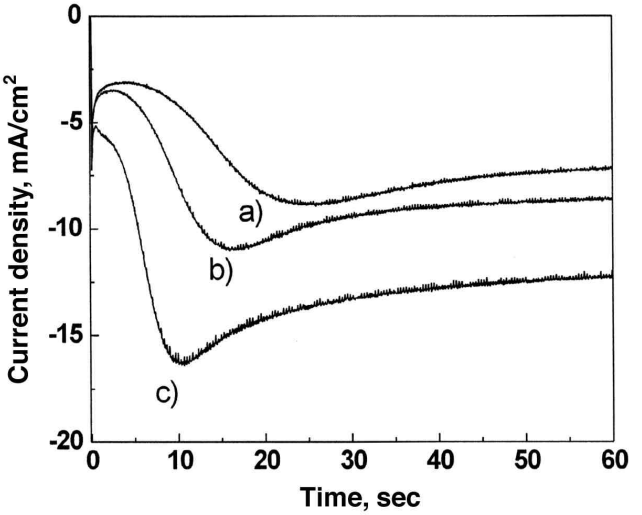


*Fig. 6—Current transients obtained at various deposition potentials of nickel on copper in 1.5 M $Ni(H_2NSO_3)_2$2 and 0.5 M $H_3BO_3$ (Bath #1): (a) -0.94 V; (b) -O.95 V; and (c) -0.97 V.*

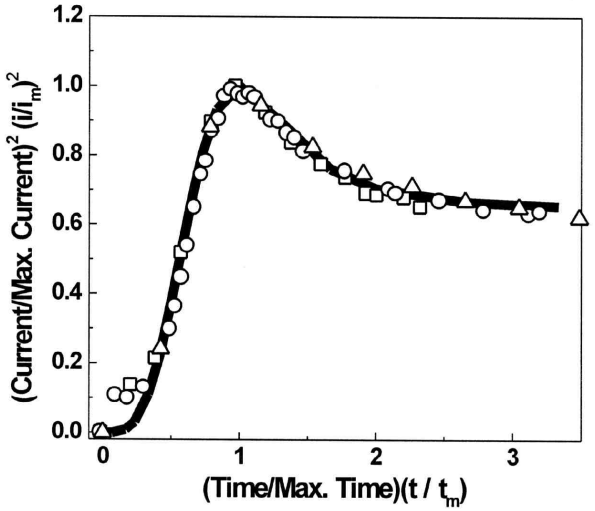


*Fig. 7—Non-dimensional current transients: solid lines = simulated transient based on instantaneous nucleation and hemispherical growth under electron transfer control; data points = experimental data from E = -0.94 (_), -0.95 (_) and -0.97 V (Δ).*

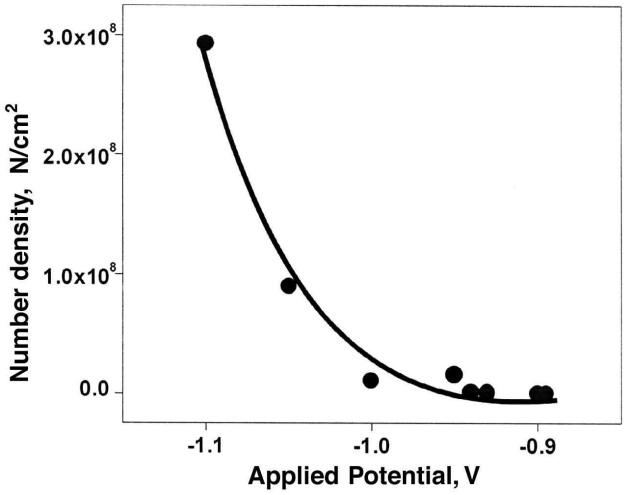


*Fig. 8—Number density of nickel nuclei as a function of deposition potential.*

and this information is essential to optimize this process.

In the case of pure nickel electrodeposition, most of the studies were conducted from Watts, sulfate, and chloride baths.[18-21] On the other hand, electrodeposition of Ni/Cu multilayers has usually been performed in sulfamate baths.[7,10,11,14-17] The texture of electrodeposited nickel depends on the electrolyte; Ross reported that nickel from sulfate baths had a (111) texture, while sulfamate baths yielded a (200) texture.[7]

Numerous kinetic studies of nickel electrocrystallization were conducted on vitreous carbon.[18,20-25] Gomez *et al*., however, used polycrystalline metals (nickel, iron, and platinum).[26] It is well known that the nature of the substrate is a very important factor in the nucleation and growth of metal thin films, eventually affecting the film's roughness and microstructure.

Kinetic studies of electrodeposition of nickel and copper from a nickel sulfamate bath in the absence and presence of copper sulfate were investigated in this study. Various current transient models were employed to determine the electrocrystallization mode and the corresponding kinetic parameters. Based on these studies, Ni/Cu multilayers were deposited potentiostatically. The relationship of the current transients to the potential pulse was examined to determine changing topography and mode of crystalline growth. X-ray diffraction and SEM were conducted to determine the crystal orientation and lamellar structure of the multilayers. The electrical resistivity and magnetoresistance were determined by the four-point-probe method.

## Experimental Procedure

Electrodeposition studies of nickel and copper were conducted with rotating disk electrodes (1500 rpm) unless specified otherwise. Copper-, platinum- and gold-sputtered silicon were utilized as working electrodes. Platinum electrodes were employed for the anodic stripping experiments. Polycrystalline copper rod (99.995% Cu) and platinum rod were embedded in Teflon with disk cross sectional areas of 0.636 mm$^2$ and 0.785 mm$^2$, respectively. For electrodeposition of Ni/Cu multilayers, flat sputtered gold silicon electrodes were employed for SEM. Before each experiment, the working electrode was mechanically polished to a mirror-bright finish with successively finer grades of $Al_2O_3$ paper (#220, 400, 600, 1200), then with wet aluminum oxide powders (1 μm and 0.05 μm) on a polishing wheel. It was then thoroughly rinsed with deionized water and degreased with isopropanol and acetone before each experiment. In the case of sputtered gold electrodes, the polishing step was omitted; they were immersed in acetone and ultrasonically cleaned in deionized water before each experiment. A Pt gauze electrode and a saturated calomel electrode (SCE), placed inside a Luggin capillary, were used as auxiliary and reference electrodes, respectively. All the given potentials are referred to SCE. The cathodic and anodic compartments were separated by a fritted glass diaphragm. Two different nickel sulfamate plating solutions were prepared in the absence (bath #1) and presence (bath #2) of 1000 ppm of $CuSO_4$. The bath composition of nickel sulfamate in the absence of $CuSO_4$ (bath #1) was 1.5 M $Ni(H_2NSO_3)_2$ + 0.5 M $H_3BO_3$. Bath #2 was the same except for the addition of 0.0157 M (1000 ppm) $CuSO_4$. All solutions were prepared with reagent grade chemicals and deionized water. The pH was maintained at 4 by addition of either NaOH or HCl. All electrochemical experiments were performed at room temperature.

Potentiostatic, cyclic voltammetry and linear sweep voltammetry were performed with a potentiostat/galvanostat

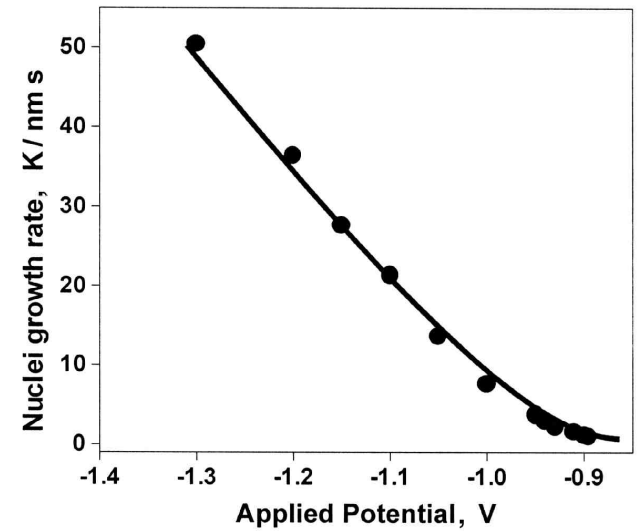


*Fig. 9—Radial hemispherically shaped growth rate as a function of deposition potential.*

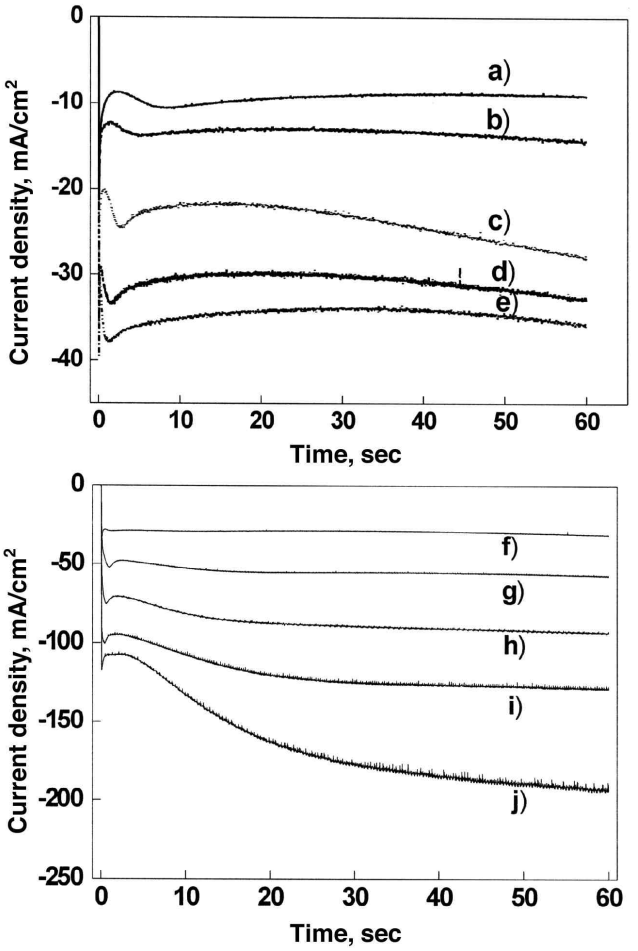


*Fig. 10—Current transients during nickel deposition on copper at various deposition potentials (Bath #2): (a) -0.93 V; (b) -0.95 V; (c) -0.98 V; (d) -0.988 mV; (e) -0.996 V; (f) -1.0 V; (g) - 1.05 V; (h) 1.10 V; (i) -1.150 V; (j) -1.20 V.*

interfaced with an IBM-compatible computer. Electrochemical measurements of nickel were performed in a copper-free bath by first setting the electrode at -0.75 V vs. SCE for 60 sec to reduce surface oxides. This reduction potential was not used for solutions containing $CuSO_4$, however.

Ni/Cu multilayer deposition was performed by applying potential pulses to a stationary electrode. The thickness and composition of magnetic and non-magnetic layers were

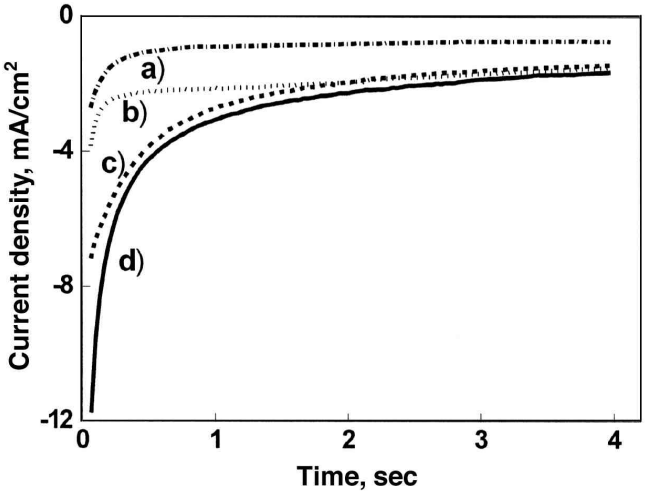


*Figure 11—Current transients during copper electrodeposition on stationary platinum in Ni sulfamate baths containing 1000 ppm of [$Cu^{+2}$] at various deposition potentials: (a) -0.15 V; (b) -0.20 V; (c) -0.40 V; (d) -0.50 V.*

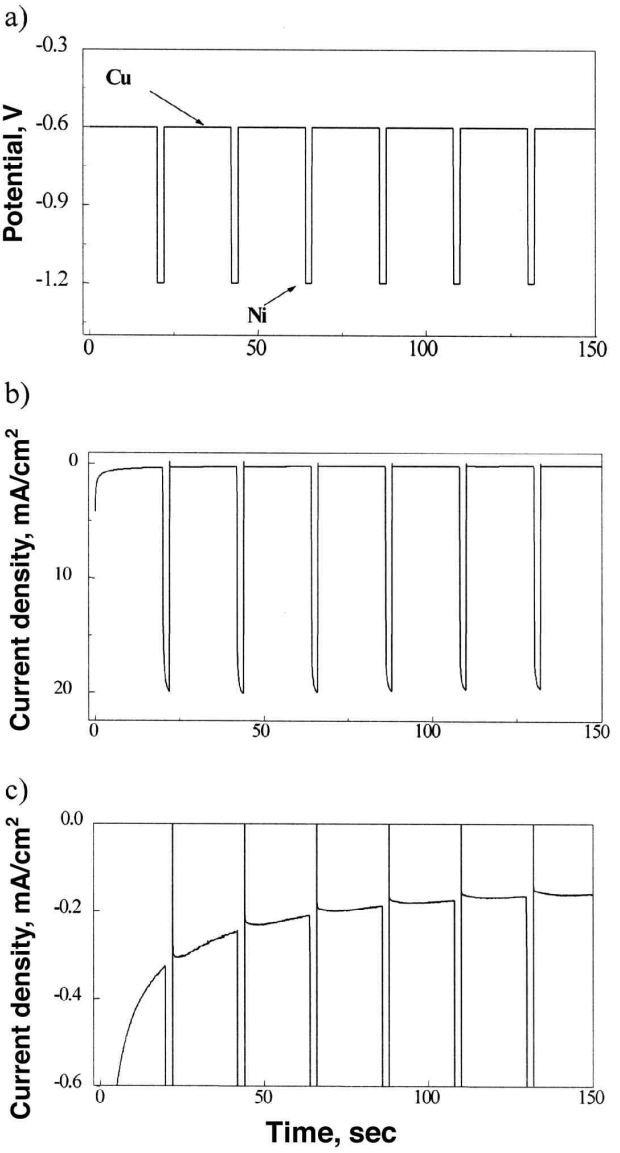


*Fig. 12—Potential waveforms and corresponding current transients during Ni/Cu multilayer deposition on stationary platinum, $E_{Ni}$ = -1.2 V, $t_{Ni}$ = 2 sec, $E_{Cu}$ = -0.6 V; $t_{Cu}$ = 20 sec: (a) potential waveforms; (b) current transients, (c) expanded scale of current transients.*

controlled by the applied potential and time. The crystal structure of the multilayers was determined by X-ray diffraction in the θ-2θ mode, using Cu-Kα radiation. To examine the cross sections of Ni/Cu multilayers, samples were cold-mounted and mechanically polished with different grit papers and alumina powder on a polishing wheel. For SEM, copper layers were slightly etched with a solution of 0.0157 M chromic acid + 0.012 M HCl + 0.36 M $H_2SO_4$ for 20 sec to distinguish between the nickel and copper layers.

A giant magnetoresistance measurement unit was constructed, consisting of a voltmeter (with 6-digit precision), current source, four-point contact and a permanent magnet (B = 1.5 kOe). The electrical resistivity (ρ) was determined by measuring the potential drop between two probes with constant current between the other two probes. Transverse magnetoresistance [$\rho_T$ - $\rho(0)/\rho_T$] was determined by measuring the difference between the electrical resistivity in the presence [$\rho_T$] and absence [$\rho(0)$] of an external magnetic field divided by the electrical resistivity in the presence of a magnetic field [$\rho_T$]. The magnetic field and current are in planes transverse to each other.

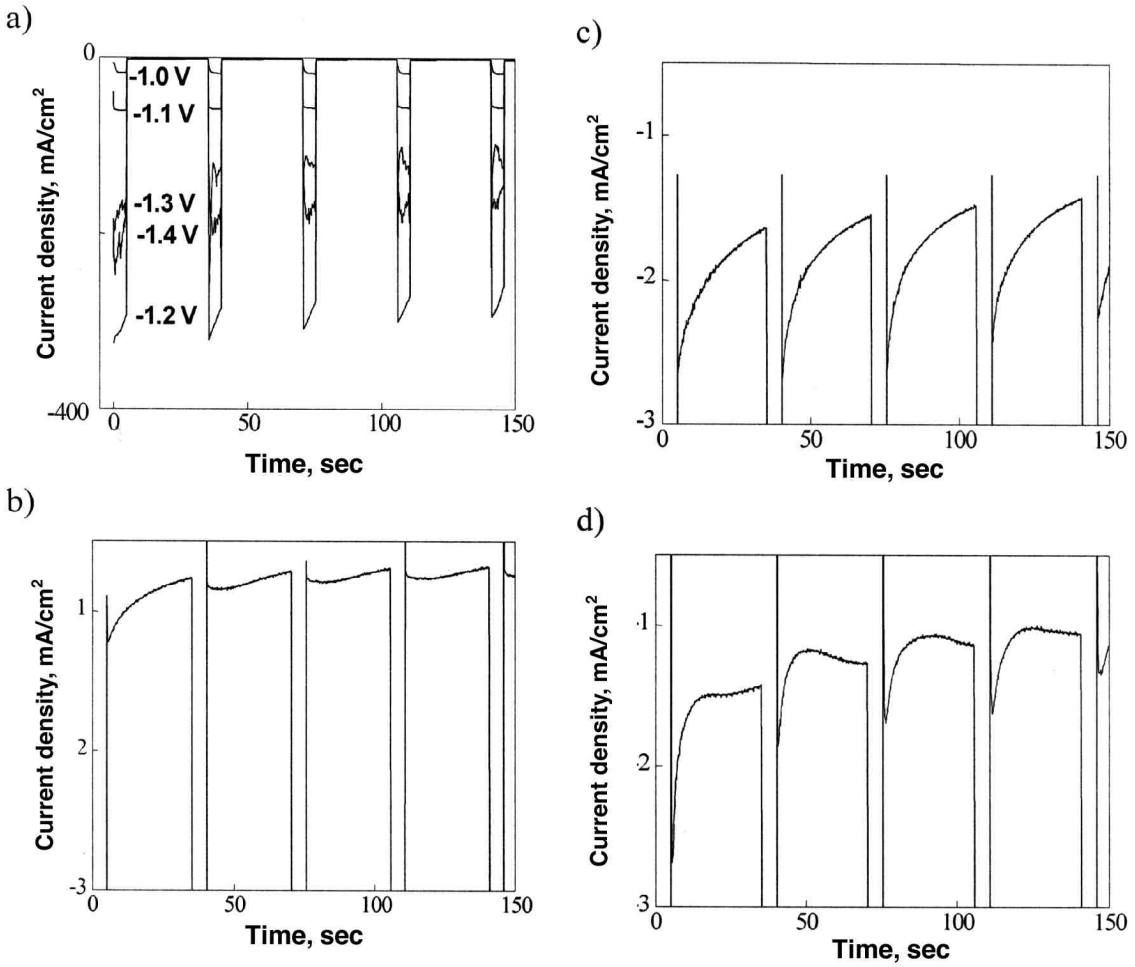


*Fig. 13—Current transients during Ni/Cu multilayer deposition on stationary platinum in sulfamate baths at various nickel deposition potentials, $E_{Cu}$ = -O.6 V, $t_{Cu}$ = 30 sec, $t_{Ni}$ = 5 sec: (a) nickel electrodeposition; (b), (c), (d) copper electrodeposition transients for $E_{Ni}$ fixed at -1.0, -1.2 and -1.4 V, respectively.*

## Results & Discussion

### Potentiodynamic Polarization

Typical polarization behavior of nickel on a copper substrate in copper-free sulfamate baths (bath #1, λ = 2 mV/sec) is shown in Fig. 1. Nickel began to electrodeposit around -0.85 V. Beyond -1.30 V, two distinct cathodic peaks ($C_1$ and $C_2$) were observed at approximately -1.35 and -1.50 V, respectively. After the second cathodic peak ($C_2$), current fluctuations were observed, as reported with vitreous carbon and palladium by others.[18,21,27,28]. Gomez *et al*. observed that at cathodic potentials beyond the first reduction peak ($C_1$), nuclei, that formed initially, quickly coalesced as a thick, cracked film. Shortly after precipitation of nickel hydroxide, a relatively small number of hemispherical Ni nuclei were formed in the cracks of the passive film.[22] This complex polarization behavior of nickel may be attributed to (1) nucleation and growth of nickel (-O.85 to -1.3 V), precipitation of nickel hydroxide (-1.3 to -1.4 V) and (2) re-nucleation and growth of nickel in the passive film cracks (-1.4 to -1.55 V). At relatively low cathodic overpotentials, the rate of hydrogen gas evolution is low, so that the local pH at the interface is approximately the same as the bulk pH. At increased cathodic potentials, however, the hydrogen evolution rate increased, causing the surface pH to rise. When the surface pH is sufficiently high, nickel hydroxide precipitates, passivating the nickel, resulting in a sharp decrease in current (peak $C_1$). With increasing sweep rate (λ), the peak current density($i_{C1}$) increases and the corresponding potential ($E_{C1}$) shifts to more negative values. Peak $C_2$ tends to disappear as λ increases and hydrogen evolution is more evident. Both $i_{C1}$ and $E_{C1}$ vary linearly with the square root of the sweep rate. Muller and Calandra *et al.* surmised that the passivation process is controlled by the electrolyte resistance in the pores of the film.[29,30]

Nickel hydride can also be electrodeposited along with nickel by incorporation of adsorbed hydrogen into the nickel matrix.[20] The amount of hydrogen incorporated in the nickel depends on the deposition process. There are two types of nickel hydrides (α and β), where α-nickel is a solid solution with a maximum atomic ratio of n = H/Ni = 0.03 and β-nickel, which has an atomic ratio of 0.6 to 1.0.[20,23] It is expected that physical properties, especially magnetic properties, would be influenced by the nickel hydride content.

Platinum was used as a substrate in place of copper to minimize substrate dissolution. Nickel was potentiodynamically deposited on Pt up to various cathodic potentials. When the potentiodynamic run was terminated at potentials less negative than $C_1$, oxidation peaks were not observed. As the cathodic potential limit increased, however, a small anodic stripping charge was obtained. Figure 2 shows an anodic stripping voltammogram of freshly electrodeposited nickel when the cathodic potential limit was set at -2.30 V with a sweep rate of 1 mV/sec. Two oxidation peaks ($A_2$ and $A_1$), at approximately -0.25 V and -0.12 V can be seen. Such anodic peaks are also evident during nickel electrodeposition in chloride and Watts baths.[24] Accordingly, $A_2$ and $A_1$ have been attributed to the oxidation of β-nickel and α-nickel hydrides.

Nickel deposited from sulfamate baths potentiostatically between -0.90 and -1.65 V for 300 sec was stripped potentiodynamically with the resulting anodic stripping voltammograms at various deposition potentials shown in Fig. 3. Oxidation peaks were not seen until deposition potentials were more negative than the potential at $C_1$. For deposition potential slightly negative to $C_1$ (-1.35 V), a single anodic peak at -0.12 V was obtained corresponding to α-nickel hydride dissolution. The anodic stripping charge at peak $A_1$ decreased as the deposition potential became more negative. After -1.43 V, a second anodic peak corresponding to β-

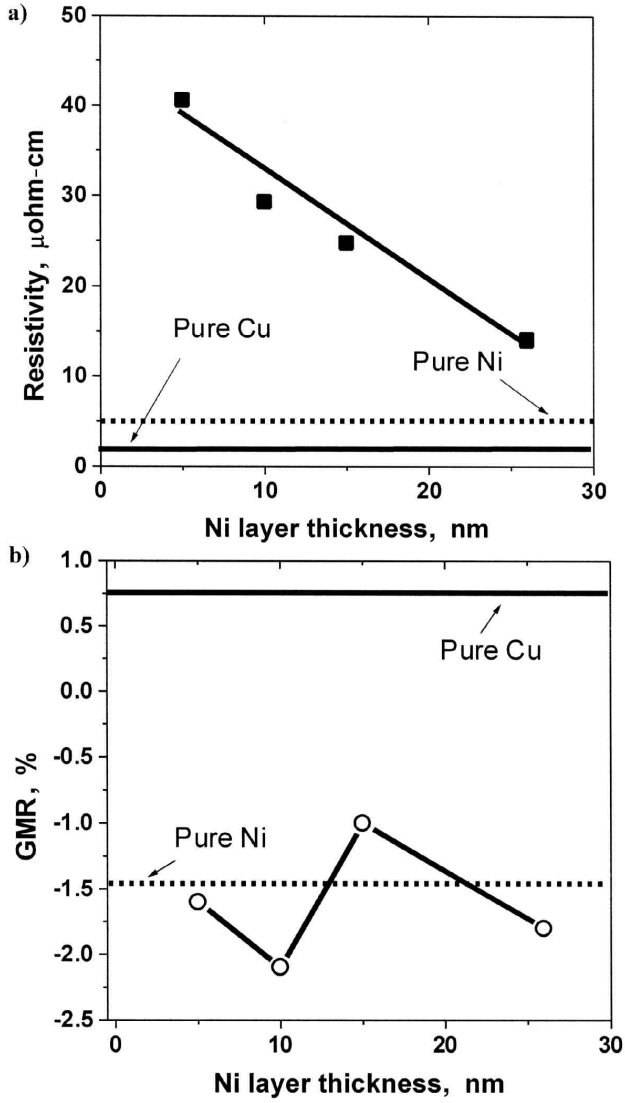


*Fig. 14—Electrical resistivity (a) and magnetoresistance (b) of Ni/Cu multilayers as a function of Ni layer thickness: $E_{Ni}$ = -1.25 V; $\delta_{Cu}$ = 2.7 nm, $E_{Cu}$ = -0.7 V.*

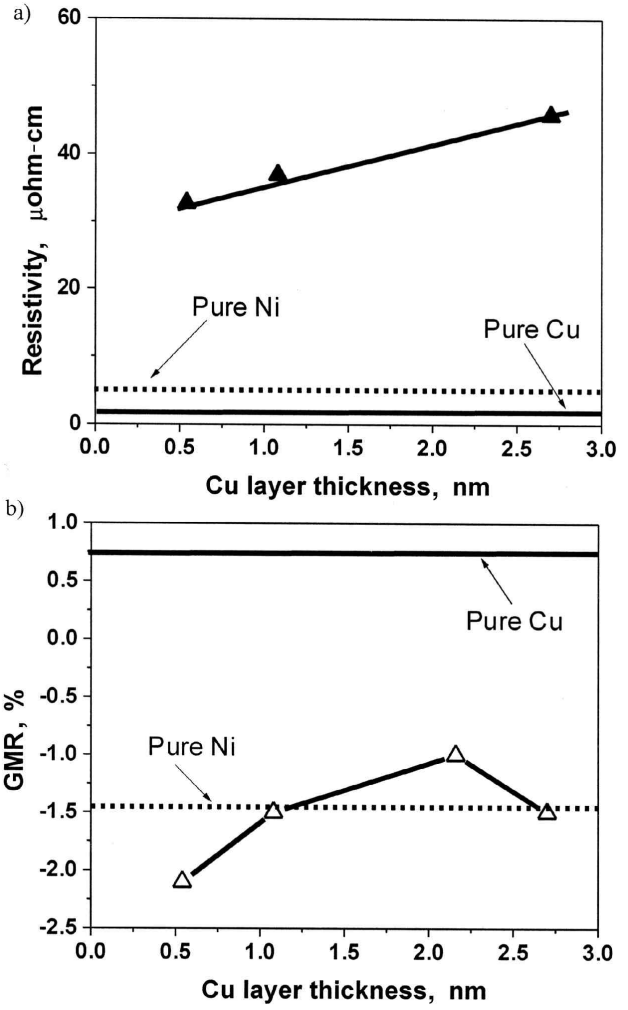


*Fig. 15—Electrical resistivity (a) and magnetoresistance (b) of Ni/Cu multilayers as a function of Cu layer thickness: $E_{Ni}$ = -1.25 V, $\delta_{Ni}$ = 5 nm; Ecu= -0.7 V.*

nickel hydride dissolution was seen at -0.25 V. After each stripping experiment, the electrode was examined with an optical microscope; electrodeposited nickel and nickel hydroxide were still seen on the platinum. These observations showed that deposited nickel could not be stripped from a sulfamate bath. At higher cathodic potentials where hydrogen evolution is significant, nickel hydrides began to codeposit with nickel because the pH at the interface had increased. β-nickel hydride formed preferentially to α-nickel hydride probably as a result of the large H/Ni ratio. Because nickel hydrides are formed by incorporation of H into the nickel crystal lattice, β-nickel hydride requires a higher content of $H_{ads}$, which can occur only at higher cathodic potentials. Figure 4 shows the anodic charge for (α- and β-nickel hydrides as a function of the deposition potential.

In a Watts bath at low cathodic potentials, Fleischmann *et al.* observed three anodic dissolution peaks, where the third peak was attributed to nickel when freshly electrodeposited nickel is anodically stripped.[20] In contrast to sulfamate baths, the presence of chloride ions in a Watts bath enables the stripping of nickel. Based on their studies, they surmised that most of the nickel was electrodeposited in a Watts bath as nickel hydride rather than nickel. In sulfamate baths, only nickel is electrodeposited at low cathodic potentials, but at sufficiently high cathodic overpotentials, small amounts of nickel hydride co-deposited with nickel.

Figure 5 shows the polarization behavior in a nickel sulfamate bath containing 1,000 ppm $CuSO_4$ (bath #2). Cathodic currents began at -0.05 V and a cathodic peak ($C_3$) can be observed at -0.08 V, followed by a current plateau of approximately -0.25 mA/cm$^2$ between -0.25 and -0.8 V. As potential sweeps went beyond -0.8 V, a steep current increase can be observed; two other distinct cathodic peaks ($C_1$ and $C_2$) are observed as in copper-free nickel sulfamate baths. The first cathodic peak ($C_3$) and the limiting current are attributed to copper deposition. Pure copper layers were deposited between -0.05 and -0.80 V, and nickel along with copper was deposited beyond -0.85 V. At more cathodic potentials, the ratio of Ni/Cu in the deposit increased. Below -1.25 V, but before $C_2$, however, the film became passivated, which may have a significant effect on multilayer properties, especially, giant magnetoresistance.

## Cathodic current transients of nickel deposition in copper-free nickel sulfamate bath (bath #1)

Potential step experiments were performed to investigate the kinetics of nickel electrodeposition in sulfamate baths. Figure 6 shows typical current transients obtained for nickel electrodeposition on copper substrates at low cathodic poten-

tials in the absence of $CuSO_4$. A common feature is the presence of a maximum current ($i_m$), followed by a current plateau ($i_L$). This maximum and current plateau vary considerably, depending on the deposition potential. The ratio of $i_m/i_L$ was always about 1.25, however. Various current transient models have been applied to simulate the nucleation and growth of nickel from sulfamate baths. Simulated results indicated that nickel nucleated instantaneously with hemispherical shape under electron transfer control. According to Bosco and Amblard, when nuclei form instantaneously with hemispherical growth controlled by electron transfer, the current passes through a maximum and reaches a plateau; the ratio of the current maximum, $i_m$, to the current plateau, $i_L$, was 1.28523.[31] From this model, the current can be related to time according the following:[31]

$$I(t) = 2nF\pi N_o K^2 t \int_0^{Kt} \exp[-\pi N(\frac{M}{\lambda} K^2 t^2 - h^2)]dh \quad (1)$$

where N is the number density of nuclei, $N_0$ is the total number density of active nuclei, K is the radial growth rate of nuclei, $\lambda$ is the density, h is the height, F is Faraday's constant, I is the current, M is the molecular weight, n is the number of equivalents per gram-atom and t is the time. The current and time at the maxima are:

$$I_m = 1.28523(\frac{nF\lambda}{M})K \quad (2a)$$

$$t_m = \frac{1.5}{(\pi NK^2)^{1/2}} \quad (2b)$$

Maxima are the result of overlapping of nuclei as deposition time increased.

The current transient was non-dimensionalized and numerically determined. Figure 7 shows good agreement between experimental and simulated current transients in non-dimensional form. Thus, the radial growth rate of single nickel crystallites can be estimated, and kinetic parameters determined. Figure 8 shows the number density of nuclei in the deposition of nickel on copper as a function of potential. The number density of nuclei increased exponentially with increase in cathodic potential. Figure 9 shows the radial growth rate of nuclei as a function of the deposition potential. The radial growth rate increased with cathodic potential from 1 nm/sec at -0.895 V to 50 nm/sec at -1.3 V.

## Cathodic current transients of nickel deposition in the presence of $CuSO_4$ (bath #2).

Typical current transients obtained for nickel deposition on copper in the presence of $CuSO_4$ (bath #2) are shown in Figure 10. A common feature is the presence of a small current peak before a monotonic change in the current up to an asymptotic value, which changes considerably as the deposition potential becomes more negative. The initial electrocrystallization stage of nickel in sulfamate baths containing $CuSO_4$ is almost the same as for Cu-free baths. The presence of copper, however, has a greater effect on the later stages of the deposition process. After a small current peak, the current increased monotonically up to the asymptotic value, but this current was greater than in the absence of $CuSO_4$.

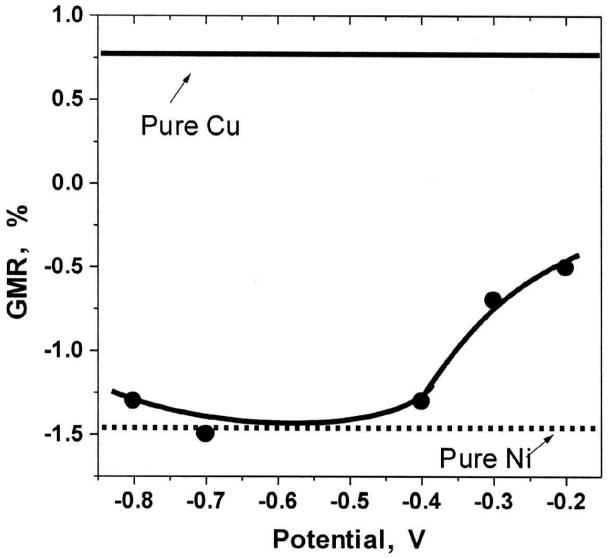


*Fig. 16—Magnetoresistance of Ni/Cu multilayers as a function of Cu deposition potential. $E_{Ni}$ = -1.25 V, $\delta_{Ni}$ = 5 nm, $\delta_{Cu}$ = 2.7 nm.*

## Cathodic current transients of copper deposition in bath #2

To examine copper electrocrystallization in nickel sulfamate baths, potentiostatic experiments were performed between -0.03 and -0.75 V. Typical current transients obtained for stationary systems are shown in Fig. 11. A general feature is the peak current immediately after the deposition potential is applied, followed by a $t^{-1/2}$ decrease in current. This behavior reflects diffusion control electrodeposition of copper.

## Cathodic Current Transient of Ni/Cu Multilayers under Potential Pulse

Based on the electrodeposition studies of copper and nickel from a sulfamate bath, we found that electrodeposition of nickel is under electron transfer and copper is under mass transfer control because of high and low metal ion concentrations, respectively, in plating bath #2. In addition, the deposition potential ranges for pure copper and nickel with small amounts of copper are -0.05 to -0.8 V and ≤ -0.85 V, respectively.

To optimize the electrodeposition of Ni/Cu multilayers and to maximize the GMR effect, deposition parameters such as the copper deposition potential ($E_{Cu}$), nickel deposition potential ($E_{Ni}$), copper layer thickness ($\delta_{Cu}$) and nickel layer thickness ($\delta_{Ni}$) were varied and the corresponding current density recorded. Figures 12a and b show typical potential waveforms and corresponding current densities vs. time for the deposition of Cu/Ni multilayers. The deposition potentials and times for copper and nickel are -0.6 V, 20 sec and -1.2 V, 2 sec, respectively, which corresponded to thicknesses of the Cu and Ni layers of 1.3 and 34.4 nm, respectively. Between -0.6 and -1.2 V, there is an immediate current response to the potential pulse, which led to sharp interfaces. Figure 12c is an expansion of 12b. The current response to the potential pulse decreased at the beginning of the first copper deposition pulse. The current transient for the second and third pulses showed an initial small increase in current followed by a decrease in current. This general shape of the observed current is independent of the deposition potential between -0.2 and -0.8 V and is attributed to mass transfer control. Copper current vs. $t^{-1/2}$ plots show a linear relationship through the origin of the plot, following the Cottrell equation.

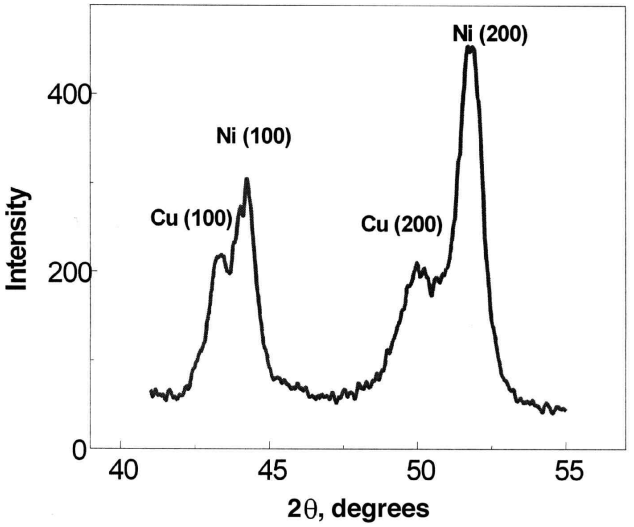


*Fig. 17—X-ray diffraction pattern of electrodeposited Ni/Cu multilayer on sputtered gold on silicon.*

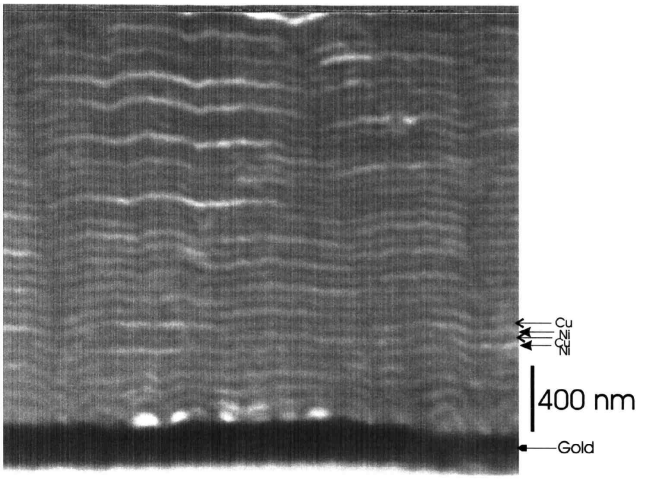


*Fig. 18—SEM micrograph of cross section of Ni/Cu multilayers. $E_{Ni}$ = -1.25 V, $\delta_{Ni}$ = 60 nm, $E_{Cu}$ = -0.7 V, $\delta_{Cu}$ = 5 nm.*

Figures 13a-d show nickel and copper electrodeposition on platinum as a function of the nickel deposition potential (-1.0 to -1.4 V ) where the copper deposition potential and time were fixed at -0.6 V and 30 sec. In Fig. 13a, the maximum current density for nickel deposition is observed at -1.2 V, which may be the result of formation of a nickel hydroxide film. Figures 13b-d show that the shape of the copper deposition current is dependent on the nickel deposition potential. When the potential is varied from -1.0 to -1.2 V, with a fixed copper deposition potential and time, the deposition current exhibits a maximum that increases as the potential increases.

Wang *et al.* observed similar behavior for a fixed nickel and copper deposition potential of -1.9 V and -0.8 V vs. SSE with variation in the nickel thickness.[15] It was surmised that when the nickel thickness was less than 10 nm, copper and nickel grew epitaxially, based on the flat current transient. For nickel thicknesses greater than 10 nm, copper deposited by three-dimensional progressive nucleation, based on the copper current peak.

## Giant Magnetoresistance (GMR) & Electrical Resistivity (ρ)

Magnetoresistance is the change of electrical resistance resulting from the presence of an external magnetic field. Magnetoresistance is dependent not only on the strength of the external magnetic field but also on the direction of the magnetic field with respect to the current. It can be measured in three different directions: longitudinal ($\Delta\rho_{ll}$) when magnetic field and current are parallel, transverse ($\Delta\rho_T$) when the magnetic field and current are perpendicular, and perpendicular ($\Delta\rho\perp$) when the magnetic field is perpendicular to the plane of the film. Magnetoresistance can be either positive or negative depending on whether electrical resistance increases or decreases in the presence of an external magnetic field. It can be categorized in three groups: ordinary magnetoresistance (OMR), anisotropic magnetoresistance (AMR) and giant magnetoresistance (GMR). Copper (non-magnetic) is OMR where $\Delta\rho > 0$. Nickel (ferromagnetic) is AMR in materials where $\Delta\rho_{ll} > 0$ and $\Delta\rho_T < 0$. GMR materials have negative MR in all field directions if $\Delta\rho < 0$ .

Six-micron-thick copper and 8-μm-thick nickel films were electrodeposited from an acid copper sulfate bath and bath #1 at 10 mA/cm$^2$, respectively. The composition of the acid copper sulfate bath was 0.8 M $CuSO_4$ + 0.5 M $H_2SO_4$ + 100 ppm NaCl + 1 vol. pct of a commercial brightener. The electrical resistivity ρ(0) and transverse MR ($\Delta\rho_T/\rho$) of electrodeposited and metallurgical nickel and copper sheet were measured by the four-point-probe method. Electrodeposited nickel and copper have ($\Delta\rho_T/\rho$) and ρ(0) at 5.5 μΩ·cm, -1.4 pct and 2.3 μΩ·cm, 0.76 pct, respectively, which are similar to metallurgical nickel and copper where ($\Delta\rho_T/\rho$) and ρ(0) of copper and nickel were 5.5 μΩ·cm, -1.4 pct and 1.7∝Ω·cm, 0.7 pct, respectively.

Giant magnetoresistance (GMR) and electrical resistivity (ρ) of Ni/Cu multilayers were functions of the Ni and Cu layer thicknesses. Figures 14a and b show the electrical resistivity and magnetoresistance of Ni/Cu multilayers as a function of nickel layer thickness while copper layer thickness was fixed at 2.7 nm. The electrical resistivity decreased monotonically from 40 to 14 μΩ·cm as the Ni layer thickness increased from 5 to 26 nm, while magnetoresistivity oscillated between -1.0 and -2.1 percent. The maximum GMR effect was observed when the nickel layer thickness was 10 nm. The oscillatory GMR effect has also been observed for other electrodeposited multilayers and is attributed to different exchange coupling of the magnetic layers.[32-34] The effect of copper layer thickness on the electrical resistivity and GMR effect was also examined by varying the copper layer thickness from 0.5 to 2 nm while keeping the nickel layer thickness at 5 nm. The electrical resistivity increased from 33 to 46 μΩ·cm (Fig. 15a), while MR decreased from -2.1 to -0.9 percent (Fig. 15b). In addition, the effect of copper deposition potential on the GMR effect of Ni/Cu multilayers was examined by varying copper deposition potentials from -0.2 to -0.8 V. The deposition potential and time for nickel were fixed at -1.2 V and 1 sec. Even though the deposition potential for Cu was varied from -0.2 to -0.8 V, the corresponding copper deposition current was essentially the same because of the limiting current. Figure 16 shows the GMR effect of Ni/Cu multilayers as a function of copper deposition potential. The GMR effect was approximately -1.5 percent between -0.4 and -0.8 V; however, the GMR effect sharply decreased when the deposition potential was more positive than -0.4 V. This might result from dissolution of the nickel during copper deposition. The cause is not yet known.

Toth *et al.* also studied the effect of copper layer thickness on the giant magnetoresistance of electrodeposited Ni/Cu

multilayers at room temperature, where they found a maximum GMR effect of -2.2 percent for Ni (3 nm)/Cu (1.5 nm) at an external magnetic field of 1.5 kOe.[35]

## X-ray Diffraction

The crystallinity and preferred orientation of Ni/Cu multilayers on (111) sputtered gold were determined by X-ray diffraction. Four sharply defined peaks, showing good crystallinity of the films, were obtained for the Ni/Cu multilayers (Fig. 17). As Ross has pointed out, the preferred orientation of nickel in sulfamate baths is (200).[7]

## SEM Micrograph

Figure 18 shows a cross sectional view of the Ni/Cu multilayers, where the deposition potential and time for Cu and Ni layers were fixed at -0.7 V, 50 sec and -1.25 V, 5 sec, respectively. To distinguish the copper from the nickel layers, copper was selectively etched. The cross sectional view shows that electrodeposited Ni/Cu multilayers have well-defined lamellar structure with nickel and copper layer thicknesses of 60 and 5 nm, respectively.

## Summary

Different electrochemical transient techniques have been employed to investigate the electrodeposition of nickel and copper in sulfamate baths. In copper-free nickel sulfamate baths, three sequential processes, nucleation and growth of nickel, precipitation of nickel hydroxide, and re-nucleation of nickel in the cracks of passive films, were indicated for cathodic potential sweeps. Nickel electrodeposited before the potential of $C_1$ was reached. The $\alpha$- and $\beta$-nickel hydrides deposited with nickel, however, when the deposition potential was more negative than $C_1$. The $\alpha$-nickel hydride began to form at potentials near the current peak, $C_1$, and $\beta$-nickel hydride was indicated near $C_2$.

By using different current transient models for the electrocrystallization process, nickel nuclei form instantaneously from copper-free sulfamate baths and grow under electron transfer control with hemispherical shape.

In copper-containing nickel sulfamate solutions, current transients of nickel changed because of copper codeposition. The copper content decreased with increasing cathodic nickel over-potentials. Pure copper can be deposited from -0.05 to -0.8 V.

Ni/Cu multilayers electrodeposited potentiostatically from sulfamate baths exhibit a fast current response leading to distinct interfaces. To obtain pure copper in Ni/Cu multilayers, the optimum deposition potential ranges from -0.4 to -0.8 V. The deposition potentials for the nickel layers were set between -1.20 and -1.25 V to minimize codeposited copper and to prevent formation of nickel hydride and nickel hydroxide films.

SEM micrographs reveal well-defined Ni/Cu multilayers. X-ray diffraction patterns show good crystallinity of Ni/Cu multilayers, where the preferred orientation was (200).

Giant magnetoresistance (GMR) and electrical resistivity ($\rho$) of Ni/Cu multilayers were determined at various Ni and Cu layer thicknesses. Electrical resistivity decreased monotonically from 40 to 14 $\mu\Omega$·cm as Ni layer thickness increased from 5 to 26 nm, while magnetoresistivity oscillated; Cu layer thickness was fixed at 2.7 nm. The electrical resistivity increased from 33 to 46 $\mu\Omega$·cm as Cu layer thickness increased from 0.5 to 2.7 nm, while GMR decreased. The GMR effect of Ni/Cu multilayers was independent of Cu deposition potential between -0.8 and -0.4 V. The GMR effect sharply decreased, however, for deposition potentials more positive than -0.4 V.

***Editor's note:*** *This work was funded in part through AESF Research Project 100.*

## Acknowledgments

Author Myung is grateful for an AESF Summer Scholarship (1997) and acknowledges helpful discussions with Dr. P.T.A. Sumodjo. Also, part of this work was done under AESF Research Project 100.

## References

1. H.Kung & T. Foecke, MRS Bulletin, **24**, 14 (1999).
2. M.N. Baibich, J.M. Broto, A. Fert, F. Nguyen Van Dau, F. Petroff, E. Etienne, G. Creuzet, A. Friederich & J. Chazales, *Phys Rev. Lett.*, **61**, 2472 (1988).
3. M. Schwartz, *Handbook of Deposition Technologies For Films and Coatings*, R.F. Bunshah, Ed., Noyes Publ., 1994; Ch. 10.
4. J.W. Dini, *Electrodeposition—The Materials Science of Coatings and Substrates*, Noyes Publ., 1992.
5. W.H. Safranek, *The Properties of Electrodeposited Metals and Alloys*," American Elsevier Publ. Co. (1974).
6. J. Yahalom & 0. Zadok, *J. Mater. Sci*. **22**, 499 (1987).
7. C.A. Ross, *Annu. Rev. Mater. Sci.,* **24,** 159 (1994) and references cited therein.
8. W. Schwarzacher & D.S. Lashmore, *IEEE Trans Magn.* **32**, 3133, (1996) and references cited therein.
9. L.H. Bennett, L.J. Swartzendruber, D.S. Lashmore, R. Oberle & U. Atzmony, *Phys. Revs.* **B40,** 4633 (1989).
10. S. Menezes & D.P. Anderson, *J. Electrochem. Soc*, **137,** 440 (1990).
11. D.M. Tench & J.T. White, *ibid*, **137**, 3061 (1990).
12. C.C. Yang & H.Y. Cheh, *J. Electrochem. Soc.*, **142,** 3034 (1995).
13. J. Yahalom, D.F. Tessier, R.S. Timsit, A.M. Rosenfield, D.F. Mitchell & P.T. Robinson, *J. Mater. Res.*, **4,** 755 (1989).
14. S.Z. Hua *et al., J. Appl. Phys.* **76,** 6519 (1994).
15. L. Wang, P. Fricoteaux, K. Yu-Zhang, M. Troyon, P. Bonhomme, J. Douglade & A. Metrot, *Thin Solid Films*, **261,** 160 (1995).
16. D.S. Lashmore & M.P. Dariel, *J. Electrochem. Soc.*, **135,** 1218 (1988).
17. D.S. Lashmore & R. Thomson, *J. Mater. Res.*, **7,** 2379 (1992).
18. E. Gomez, C. Miller, W.G. Proud, E. Valles, *J. Appl. Electrochem.*, **22,** 872 (1992).
19. M.Y. Abyaneh, *Tran. Inst. Metal Fin.*, **69,** 70 (1991) and references cited therein.
20. M. Fleischmann & A. Saraby-Reintjes, *Electrochim. Acta*, **29**(1) 69 (1984).
21. S.G. Garcia, D. Salinas, C. Mayer, J.R. Vilche, H.-J. Pauling, S. Vinzelberg, F. Staikov & W.J. Lorenz, *Surf Sci.*, **316,** 143 (1994).
22. E. Gomez, C. Muller, R. Pollina, M. Sarret & E. Valles, *J. Electroanal. Chem.*, **333** 47 (1992).
23. R. Albalat, E. Gomez, C. Muller, M. Sarret, E. Valles, *J. Appl. Electrochem.*, **21,** 709 (1991).
24. W.G. Proud, E. Gomez, E. Saffet, E. Valles & C. Muller, *ibid*, **25,** 770 (1995).
25. Chr. Bozhkov, Chr. Tzetkova, St. Rashkov, Antoni.

Budniok & Adam Budniok, *J. Electroanal. Chem*., **296**, 453 (1990).
26. E. Gomez, R. Pollina & E. Valles, *ibid*, **386,** 45 (1995).
27. R. Ragauskas & V. Lenksminas, *Sov. Electrochem.*, **24**, 675 (1988).
28. Z. Chen, J. Li & E. Wang, *J. Electroanal. Chem*., **373,** 83 (1994).
29. W.J. Muller, *Trans. Faraday Soc.*, **27,** 737 (1931).
30. A.J. Calandra *et al*., *Electrochim. Acta*, **19,** 901 (1974).
31. E. Bosco & S.K. Rangarajan, *Electrochim. Acta,* **134,** 213 (1982).
32. D.S. Lashmore, Y. Zhang, S. Hua, M.P. Dariel, L. Swartzendruber & L. Salamanca-Riba, *Proc. Electrochem. Soc.,* **PV94-6**, 205 (1994).
33. S.Z. Hua, D.S. Lashmore, L. Salamanca-Riba, W. Schwarzacher, L.J.
Swartzendruber, R.D. McMicheal, L. H. Bennett & R. Hart, *J. Appl. Phys*. **76,** 6519 (1994).
34. K. Bird & M. Schlesinger, *J. Electrochem. Soc*.,**142**, L65 (1995).
35. J. Toth, L.F. Kiss, E. Toth-Kadar, A. Dinia, V. Pierron-Bohness, & I. Bakonyi, *J. Magn. Mater* (1999).

## About the Authors

*Dr. Nosang V. Myung is a research engineer at UCLA, from which he holds BS, MS and PhD in chemical engineering. His current research interests are in electrodeposition of nano-structured hard and soft magnetic thin films, rare earth/transition-metal alloys, polymer-metal lamellar composites and iron group alloys with vanadium, tungsten and molybdenum. He also has interests in corrosion electrochemistry of high-strength aluminum and titanium alloys, as well as iron- and nickel-based alloys.*

*Prof. Ken Nobe* is a faculty member in the Dept. of Chemical Engineering at UCLA, 405 Hilgard Ave., Los Angeles, CA 90095-1592. He has been employed in this capacity since receiving his PhD degree in 1956. Prof. Nobe's research interests are in electrochemistry and catalysis.*

** To whom correspondence should be addressed.*